Research Square

Preprints are preliminary reports that have not undergone peer review.
They should not be considered conclusive, used to inform clinical practice,
or referenced by the media as validated information.

The plasma extracellular vesicle lipidome reveals sex-specific acyl-chain signatures in patients with alcohol use disorder

Blanca Martín-Urdiales
University of Valencia
Miguel Marcos
University Hospital of Salamanca
María Pascual
maria.pascual@uv.es

University of Valencia

Research Article

Keywords: Lipidomics, acyl-chain length, total chain unsaturation, extracellular vesicles, plasma, alcohol use disorder

Posted Date: November 18th, 2026

DOI: https://doi.org/10.21203/rs.3.rs-11521415/v1

License: This work is licensed under a Creative Commons Attribution 4.0 International License.
Read Full License

Additional Declarations: No competing interests reported.

Abstract

Alcohol use disorder (AUD) is associated with profound metabolic alterations, but the impact of chronic alcohol consumption on the structural lipid composition of extracellular vesicles (EVs) remains poorly understood. This study investigated sex-specific differences in the acyl-chain length and degree of unsaturation of EV lipids in AUD. Plasma-derived EVs were isolated from AUD patients and healthy individuals. Lipidomic profiling was performed by LC-MS/MS, and differential abundance analyses, as well as structural lipid features including total acyl chain length and unsaturation, were assessed using the *lipidr* package. Male AUD patients exhibited a depletion of highly unsaturated lipid species consistent with increased oxidative vulnerability and membrane remodeling, whereas females showed an enrichment of long-chain and polyunsaturated lipids suggestive of distinct metabolic adaptations (e.g., sex hormone-related differences in polyunsaturated fatty acid metabolism). Furthermore, since membrane lipid composition governs EV stability, biodistribution, and intercellular communication, the marked reorganization of sphingolipid and glycerophospholipid species may alter membrane architecture and vesicle function, contributing to sex-specific differences in EV biology under alcohol exposure. These patterns suggest differential regulation of fatty acid elongation, desaturation, and sphingolipid metabolism in response to chronic alcohol exposure. Collectively, the present data highlight EV lipid remodeling as a potential mechanism involved in alcohol-induced pathological processes and provide a framework for future studies investigating the role of EVs in AUD pathophysiology.

Highlights

Male AUD patients exhibited a depletion of highly unsaturated lipid species in plasma-derived EVs, consistent with increased oxidative vulnerability and membrane remodeling.

Female AUD patients showed an enrichment of long-chain and polyunsaturated lipids in plasma-derived EVs, suggestive of distinct metabolic adaptations.

EV lipid remodeling may disrupt EV stability, biodistribution, and intercellular communication, contributing to AUD pathology.

Background

Alcohol use disorder (AUD) is a chronic relapsing condition characterized by compulsive alcohol consumption, loss of control over alcohol intake, and the emergence of negative emotional states during abstinence [1]. AUD encompasses a broad spectrum of clinical manifestations and contributes substantially to the global burden of disease, accounting for approximately three million deaths annually worldwide. Excessive alcohol consumption is associated with a wide range of adverse health outcomes, including alcohol-associated liver disease, hepatocellular carcinoma, cardiovascular complications, neurological impairment, and psychiatric disorders [2]. Given its considerable impact on public health and healthcare systems, there is increasing interest in identifying biomarkers that improve the

understanding of AUD pathophysiology and facilitate the development of noninvasive diagnostic and prognostic tools [3].

Extracellular vesicles (EVs) are nanosized membrane-bound particles released by virtually all cell types into the extracellular milieu. EVs mediate intercellular communication through the transfer of proteins, nucleic acids, lipids, and other bioactive molecules, thereby influencing numerous physiological and pathological processes [3–5]. Owing to their stability in biological fluids and their ability to reflect the molecular state of their cells of origin, EVs have emerged as promising biomarkers for a variety of diseases, including alcohol-associated liver injury and neuroinflammatory disorders [5]. While considerable attention has been devoted to the protein and nucleic acid cargo of EVs, the biological significance of their lipid composition remains comparatively underexplored. Recent evidence has shown that ethanol exposure induces sex-dependent alterations in the lipid cargo of circulating EVs, suggesting that EV-associated lipids may contribute to alcohol-induced inflammatory responses and represent sensitive indicators of alcohol-related pathophysiological changes [6, 7].

Lipids are fundamental structural and functional components of cellular and EV membranes, participating in membrane organization, signal transduction, energy homeostasis, and inflammatory regulation. Advances in mass spectrometry-based lipidomics have enabled the comprehensive characterization of hundreds to thousands of lipid species in biological samples, providing unprecedented insight into lipid metabolic pathways and their dysregulation in disease [8, 9]. Lipids belonging to the same class can differ markedly in acyl-chain length and degree of unsaturation, properties that critically influence membrane fluidity, curvature, permeability, vesicle biogenesis, and cell signaling [10–13]. Experimental evidence has demonstrated that variations in acyl-chain composition alter the biophysical behavior of membrane lipids and modulate cellular responses, emphasizing the importance of lipid architecture beyond lipid class quantification [10–12]. Given the central role of membrane lipids in EV formation and function, characterization of acyl-chain structural features may reveal biologically meaningful signatures that remain undetected by conventional lipidomic approaches.

Considering the emerging evidence that alcohol exposure alters EV lipid cargo [6, 7], the underexplored biological significance of EV lipid structural features, and the critical role of acyl-chain composition in membrane dynamics and cellular function, the aim of the present study was to characterize the acyl-chain length and degree of saturation of lipid species present in plasma-derived EVs from patients with AUD and healthy controls. In this context, we found that chronic alcohol consumption was associated with sex-dependent remodeling of the lipid composition of circulating EVs. Male patients with AUD exhibited a depletion of long-chain and highly unsaturated lipid species, whereas females showed an enrichment of these lipids. These findings suggest differential regulation of lipid metabolism in response to chronic alcohol exposure and may have implications for EV function and AUD pathophysiology.

Methods

Human subjects

The present study was conducted using plasma samples from the same cohort previously characterized by Perpiñá-Clérigues et al. [7]. The study population comprised 11 patients with alcohol use disorder (AUD), diagnosed according to DSM-5 criteria, including six males and five females, who were recruited through the Alcoholism Unit of the University Hospital of Salamanca, Spain. The median ages of the male and female AUD patients were 47.83 and 40.00 years, respectively. All AUD patients reported an alcohol intake of ≥ 90 g of ethanol per day prior to study inclusion.

Participants had normal prothrombin time, hemoglobin, and serum albumin concentrations and tested negative for hepatitis B surface antigen and hepatitis C antibodies. Individuals with concomitant acute or chronic conditions that could interfere with the study outcomes, as well as those with polydrug abuse, were excluded. Advanced liver disease was ruled out based on clinical examination, biochemical parameters, and liver ultrasonography. Participants presenting clinical signs of chronic liver disease, such as cutaneous manifestations, hepatosplenomegaly, gynecomastia, testicular atrophy, or muscle wasting, were excluded if these findings were accompanied by ultrasonographic abnormalities other than steatosis or by liver transaminase levels exceeding two- to three-fold the upper reference limit.

The control group consisted of 12 healthy volunteers, six males and six females, who reported an alcohol intake of < 15 g/day. All control participants exhibited normal liver function and standard hematological and biochemical parameters. The median ages of the male and female control participants were 39.50 and 45.50 years, respectively.

All participants provided written informed consent before inclusion in the study. The study protocol was approved by the Ethics Committee of the University Hospital of Salamanca, Spain. Peripheral blood samples were collected into heparin-containing tubes between 9:00 and 10:00 AM under fasting conditions. Plasma was immediately separated, snap-frozen in liquid nitrogen, and stored at − 80°C until further processing. Samples were subsequently used for biochemical analyses and EV isolation; the biochemical data were previously described in Perpiñá-Clérigues et al. [7].

EV isolation from human plasma and EV characterization

EVs were obtained from plasma using the Total Exosome Isolation Kit (catalog no. 4484450, Invitrogen, USA) according to the manufacturer's protocol. 250 µL of plasma was processed for EV isolation. The resulting EV preparations were collected and maintained at − 80°C until further analysis. The isolated EVs were subsequently used for either lipid extraction or vesicle characterization. For morphological characterization, freshly isolated EVs were fixed in 2% paraformaldehyde and processed according to the procedure previously reported [14]. Samples were examined by transmission electron microscopy (TEM) using an FEI Tecnai G2 Spirit microscope (FEI Europe, Eindhoven, The Netherlands) equipped with a Morada digital camera (Olympus Soft Image Solutions GmbH, Münster, Germany). EV concentration and size distribution were additionally determined by nanoparticle tracking analysis using a NanoSight NS300 system (Malvern/NanoSight Ltd., Minton Park, U.K.), following the methodology described previously [14].

Lipid extraction

For lipidomic analysis, an equal volume of EV suspension (0.2 mL per sample) was subjected to lipid extraction using a modified Folch procedure. Following phase separation, the lower organic fraction containing the lipids was recovered and evaporated under a nitrogen stream. The dried extracts were stored at − 80°C until analysis. Prior to liquid chromatography-tandem mass spectrometry (LC-MS/MS), the lipid residues were reconstituted in isopropanol. Samples were subsequently analyzed under both positive- and negative-ionization conditions.

LC-MS/MS analysis

For the initial quadrupole time-of-flight (QTOF) MS acquisition, a pooled lipid extract generated by combining aliquots from the 36 samples included in the study (four experimental conditions with nine biological replicates each) was analyzed using an iterative MS/MS strategy. Liquid chromatographic separation and automated MS/MS acquisition were performed following previously published protocols [6, 7] with minor modifications.

Chromatographic analyses were carried out on an Agilent 1290 Infinity LC system coupled to an Agilent 6550 Accurate-Mass QTOF mass spectrometer (Agilent Technologies, Santa Clara, CA, USA). Ionization was achieved using an electrospray interface equipped with Jet Stream Technology. The instrument was operated in positive-ion mode at 3500 V and in negative-ion mode at 3000 V, using the high-sensitivity setting. The electrospray source was maintained at a gas temperature of 200°C, with a drying gas flow of 12 L/min, a nebulizer pressure of 50 psi, a sheath gas temperature of 300°C, and a sheath gas flow of 12 L/min.

Chromatographic separation was performed on an InfinityLab Poroshell 120 EC-C18 column (3.0 × 100 mm, 2.7 µm; Agilent, Santa Clara, CA, USA). The mobile phase consisted of solvent A, containing 10 mM ammonium acetate and 0.2 mM ammonium fluoride in water/methanol (9:1, v/v), and solvent B, containing 10 mM ammonium acetate and 0.2 mM ammonium fluoride in acetonitrile/methanol/isopropanol (2:3:5, v/v/v). The optimized gradient started at 70% B at 0 min and was maintained until 1 min, followed by an increase to 86% B at 3.5 min. This composition was maintained until 10 min, after which the proportion of solvent B was increased to 100% at 11 min and maintained until 17 min. The column temperature was set to 50°C and the flow rate was kept constant at 0.6 mL/min. An injection volume of 5 µL was used for both ionization modes.

Mass spectrometric data were acquired with Agilent MassHunter Workstation software. LC/MS Data Acquisition B.10.1 (Build 10.1.48) was operated in automated MS/MS acquisition mode. Within the 300–1700 m/z range, the three most abundant ions with charge states of 1–2 were selected for fragmentation when their intensity exceeded 5,000 counts and 0.001%. The quadrupole was operated under narrow isolation conditions with a resolution of 1.3 m/z. MS/MS spectra were collected over the

50–1700 m/z range until either a cumulative signal of 25,000 counts was reached or the maximum accumulation time of 333 ms was attained.

Continuous internal mass calibration was applied throughout the analyses to maintain mass accuracy. For positive-ion measurements, m/z 121.050873 and 922.009798 were used as reference ions, whereas m/z 119.03632 and 980.016375 served as calibrants in negative-ion mode. In addition, all-ion MS/MS measurements were performed on individual samples using an acquisition rate of three spectra per second and four collision-energy segments (0, 10, 20, and 40 eV), as implemented in the Agilent Technologies (2013) acquisition method.

Lipid annotator database

As an initial step in the lipidomics workflow, five sets of five iterative MS/MS files generated from pooled human cell extracts were processed using Lipid Annotator software. Lipid annotation was performed with Lipid Annotator [15] which integrates Bayesian scoring, probability-density calculations, and non-negative least-squares fitting to compare experimental MS/MS spectra against a theoretical lipid library. The library was based on a modified version of LipidBlast developed by Kind et al. (2015) [16].

Agilent MassHunter Lipid Annotator version 1.0 was subsequently employed for the remaining data-processing steps. Unless otherwise specified, the default software parameters were retained. For positive-ion analyses, precursor ions were restricted to [M + H] + and [M+NH4]+, whereas [M − H] − and [M + HAc−H]− were considered for negative-ion measurements. Exported lipid annotations were subsequently managed and curated using the Agilent MassHunter Personal Compound Database and Library (PCDL) Manager version B.08 SP1.

Lipid identification

The lipid-specific PCDL databases generated during annotation were subsequently used for targeted, batch-wise feature extraction from the 36 all-ion MS/MS data files using Agilent MassHunter Qualitative Analysis version 10.0. The standard “Profinder - Lipids.m” method was adapted within MassHunter Qualitative software according to the modifications previously described by Sartain et al. [17]. Feature detection and putative identification were performed using the Find by Formula (FbF) algorithm implemented in MassHunter Qualitative Analysis. This modified FbF workflow is compatible with all-ion MS/MS data. Initially, mass features detected in the low-energy channel were matched against compounds in the corresponding PCDL database according to their m/z values, generating a preliminary list of candidate lipid identifications. The corresponding MS/MS fragment ions recorded in the high-energy channel were then compared with the theoretical fragments contained in the PCDL database to provide additional evidence for lipid identification.

Precursor and product ions were extracted as chromatographic ion traces and assessed according to their coelution characteristics. A coelution score was calculated by the software based on several

chromatographic and signal parameters, including abundance, peak-shape symmetry, peak width, and retention time. The resulting feature list was manually reviewed in MassHunter Qualitative Analysis, and features that did not meet the required quality criteria were discarded. Finally, the MassHunter Qualitative Analysis results and the retained, quality-controlled features were exported in .cef format for subsequent data processing and statistical analysis.

Bioinformatic analyses

Bioinformatic processing of the lipidomic dataset was carried out in R (version 4.1.2; R Development Core Team). Figure 1 summarizes the study design and the analytical workflow employed. Comparative analyses were performed to evaluate differences between male and female individuals diagnosed with AUD and healthy control participants (AUD vs. Control).

Data preprocessing

Data preprocessing comprised feature filtering, normalization of the lipid abundance matrix, and exploratory data assessment. Raw output files generated with MassHunter Qualitative (.cef format) were imported into Mass Profiler Professional (Agilent Technologies) for subsequent statistical analyses. Features were filtered according to their detection frequency, keeping only those present in all replicates of at least one study group.

Normalization was performed by applying a 75th-percentile shift method, followed by baseline correction using the median value across all samples. This procedure helped reduce technical variability and eliminate atypical signal patterns [17]. After normalization, datasets obtained in positive and negative ionization modes were annotated accordingly and merged into a unified data frame.

To facilitate downstream bioinformatic analyses, lipid annotations were harmonized following standardized nomenclature conventions compatible with the *lipidr* package in R [18]. Exploratory analyses included hierarchical clustering and principal component analysis (PCA) to evaluate abundance distributions and identify potential batch-related effects.

To further reduce the influence of batch effects on differential abundance testing, samples displaying atypical behavior were removed. Outliers were defined as observations falling below Q1 − 1.5 × IQR or above Q3 + 1.5 × IQR, where IQR corresponds to the interquartile range.

Differential lipid abundance

Differential abundance was assessed using the *lipidr* R package [18], with p-values adjusted by Benjamini & Hochberg (BH) procedure [19]. Two independent analyses were performed: one comparing male AUD patients with healthy male controls (IM comparison), and another comparing female AUD patients with healthy female controls (IF comparison). The log2 fold change (LFC) statistic indicated whether lipid

abundance was greater in AUD patients (positive LFC) or controls (negative LFC). The lipids showing significant differential abundance (adj.P.Val < 0.05) in each comparison are reported in **Additional file 1**, together with their total chain length and total number of double bonds and are separated according to their LFC.

Class annotation

Classification of lipid species was carried out using the RefMet (Metabolomics Workbench) [20, 21] and LIPID MAPS [22] database. **Additional file 2** summarizes the abbreviations used throughout the study and provides the hierarchical classification of all lipids identified in the samples, including their superclass, main class, and subclass.

Lipid structure analysis

Structural lipid characteristics, including total fatty acyl chain length (number of carbon atoms) and degree of unsaturation (number of double bonds), were calculated using the *lipidr* package in R [18]. This software derives structural attributes directly from lipid annotations, extracting information on the cumulative carbon content and total unsaturation of each lipid species.

Differences in the distribution of these structural features between AUD and control groups were assessed using functions available within *lipidr*. To investigate the association between lipid regulation and structural composition, locally estimated scatterplot smoothing (LOESS) models were fitted to evaluate the relationship between log2 fold-change (LFC) values and either acyl chain length or unsaturation level.

For univariate analyses, differentially regulated lipid species were identified using moderated t-statistics as implemented in the *lipidr* analytical framework.

Web platform

A publicly accessible web application (https://bioinfouvcipf.shinyapps.io/EVLipoStruct-AUD/) has been developed to provide detailed documentation of the computational approaches used in this study. The platform allows users to examine the outcomes of all statistical analyses, interactively explore the dataset, and investigate specific lipid signatures of interest.

By offering open access to the results, this resource promotes transparency and data dissemination while supporting further research initiatives. In addition, it serves as a valuable tool for generating new hypotheses and facilitating the identification of previously unrecognized patterns within the lipidomic data.

Results

Lipidomics data exploration of plasma EVs isolated from AUD patients

Prior to lipidomic profiling, plasma EVs isolated from healthy controls and patients with AUD were characterized by transmission electron microscopy (TEM), and nanoparticle tracking analysis (NTA) (Fig. 2). TEM imaging revealed nanoscale vesicles with the characteristic morphology and size expected for exosomes, with diameters of approximately 100 nm (Fig. 2A). In agreement with these observations, NTA demonstrated a predominant particle size distribution within the 100–200 nm range, consistent with plasma EV populations (Fig. 2B).

Lipidomic analyses were performed on plasma EV samples obtained from female and male individuals with AUD and their respective healthy controls. Using LC-MS/MS-based profiling, we investigated structural lipid alterations across the four experimental groups defined by sex and alcohol consumption status. Differential abundance analysis was conducted with the *lipidr* package to identify lipid species significantly altered between AUD and control groups within each sex comparison (IF and IM). The results of the differential abundance analysis have been previously reported by Perpiñá-Clérigues et al. (2024) and are summarized in Fig. 2C. Briefly, both increased (LFC > 0) and decreased (LFC < 0) lipid species were detected and categorized according to lipid superclass. The complete dataset is available through the associated web platform (https://bioinfouvcipf.shinyapps.io/EVLipoStruct-AUD/)

Sex-based differences in the acyl-chain length and saturation of fatty acids in plasma EVs isolated from AUD patients

In the fatty acid (FA) class, sex-stratified analysis revealed distinct structural remodeling associated with AUD. In males (IM), FA species containing 16–20 carbon atoms showed predominantly negative log fold changes (LFC < 0), indicating a relative depletion of medium-chain FAs in AUD patients compared with controls. In contrast, females (IF) exhibited increased abundance of longer-chain FA species (20–22 carbons; LFC > 0), suggesting sex-specific regulation of elongated fatty acids in AUD (Fig. 3).

Regarding unsaturation, both groups of AUD patients displayed comparable trends in FA species with 0–4 double bonds. However, highly unsaturated FAs (5–6 double bonds) showed opposite patterns, with decreased levels in IM and increased levels in IF, indicating divergent regulation of polyunsaturated fatty acids between sexes (Fig. 3).

Sex-based differences in the acyl-chain length and saturation of sphingolipids in plasma EVs isolated from AUD patients

Within the sphingolipid superclass, ceramides (Cer) displayed clear sex-specific patterns. In IF, Cer species with 34–40 carbons were decreased, while in IM the decrease was mainly observed in longer-chain species (38–40 carbons). Conversely, short-chain ceramides (< 36 carbons) were increased in IM. Unsaturation analysis revealed opposite regulation of saturated ceramides, which increased in IM and decreased in IF (Fig. 4A).

Furthermore, sphingomyelins (SMs) showed reduced abundance of species with > 36 carbons in IM and < 40 carbons in IF. Regarding unsaturation, IM exhibited decreased levels of polyunsaturated SMs (> 2

double bonds), whereas IF showed decreased levels in species with 2–3 double bonds but increased abundance in highly unsaturated SMs (4–5 double bonds), indicating sex-dependent remodeling of sphingomyelin saturation states (Fig. 4B).

Sex-based differences in the acyl-chain length and saturation of phospholipids in plasma EVs isolated from AUD patients

Within glycerophospholipids, phosphatidylcholine (PC) species with 34–40 carbons were decreased in both IM and IF. Additionally, IF showed reduced abundance of short-chain PCs (< 26 carbons). In terms of unsaturation, IF exhibited decreased levels of PCs with four double bonds, whereas IM showed a more complex pattern, with decreased abundance in PCs containing four to five double bonds and increased levels in more highly unsaturated species (≥ 6 double bonds), suggesting differential remodeling of highly unsaturated PCs between sexes (Fig. 5A).

Phosphatidylethanolamines (PEs) also showed marked sex-specific patterns. In IM, PE species with 36–38 carbons were reduced, whereas shorter or longer species showed increased abundance. In IF, PE species with < 36 carbons were increased, while those with > 38 carbons were decreased, and species within the 36–38 carbon range remained largely unchanged. These patterns indicate opposite regulation of medium- and long-chain PEs between sexes. Regarding unsaturation, IM showed decreased levels in PE species with 1–2 double bonds and increased levels in those with 3–4 double bonds, while IF displayed the opposite trend, with increased abundance of low-unsaturation PEs and reduced levels of species containing three double bonds (Fig. 5B).

Regarding the lysophosphatidylcholines (LPCs), both IM and IF showed reduced abundance of short-chain species (< 16 carbons). However, longer-chain LPCs (> 16 carbons) increased in IM, whereas they remained unchanged in IF. Regarding unsaturation, IM showed increased levels of monounsaturated LPCs and those with 4–5 double bonds, but decreased levels in species with three double bonds. In IF, LPCs with a single double bond were reduced, while other unsaturation states remained largely unchanged, suggesting a weaker overall remodeling of LPC unsaturation in females (Fig. 5C).

Sex-based differences in the acyl-chain length and saturation of triacylglycerols in plasma EVs isolated from AUD patients

In triacylglycerides (TGs), both comparisons showed similar behavior for species containing fewer than 58 carbon atoms. Nevertheless, TGs with longer chains (> 58 carbons) exhibited opposite trends, with decreased abundance in IM and increased abundance in IF, suggesting sex-dependent regulation of very-long-chain neutral lipids. Polyunsaturated TGs (> 5 double bonds) were reduced in IM, whereas IF showed an increase in TGs with 5–8 double bonds (Fig. 6).

Discussion

The present study reveals, for the first time, sex-dependent alterations in EV lipid structural trends, characterized by differences in acyl-chain length and lipid unsaturation patterns, in individuals with AUD. While male patients exhibited a relative depletion of long-chain and highly polyunsaturated lipid species, particularly within the fatty acid (FA), sphingomyelin (SM), and triacylglycerol (TG) classes, females showed a consistent enrichment of long-chain and polyunsaturated species. These findings are consistent with growing evidence indicating that alcohol-induced lipid dysregulation is strongly influenced by biological sex [6, 7, 23]. Recent lipidomic analyses of plasma EVs from AUD patients demonstrated distinct sex-dependent alterations in lipid metabolic networks, with females displaying a predominant dysregulation of phosphatidylcholine and lysophosphatidylcholine metabolism, whereas males exhibited a more pronounced disruption of ceramide and sphingomyelin pathways [7, 23]. Similarly, experimental models of chronic ethanol exposure have identified sex as a major determinant of EV lipid composition and membrane-associated lipid ontology signatures [24]. Collectively, these observations support the existence of sex-specific lipid metabolic responses to chronic alcohol exposure and highlight the importance of considering sex as a critical biological variable in EV-based studies of AUD.

Beyond these class-specific trends, the depletion of highly unsaturated species in males suggests a role for enhanced lipid peroxidation under chronic alcohol exposure. The metabolism of ethanol and its byproduct acetaldehyde promotes ROS generation, thereby contributing to oxidative stress and oxidative damage to cellular lipids [25]. Consistent with this mechanism, individuals with AUD exhibit elevated levels of lipid peroxidation products together with impaired antioxidant defenses [26]. Polyunsaturated fatty acids (PUFAs) are particularly susceptible to ROS-mediated peroxidation owing to their high degree of unsaturation, resulting in the formation of lipid hydroperoxides and secondary reactive aldehydes [27]. Therefore, the reduction of FA species containing five to six double bonds, together with the depletion of highly unsaturated PCs, SMs and TGs observed in males, could result from preferential oxidation and subsequent removal of these molecular species. Beyond their susceptibility to oxidative degradation, very-long-chain n-3 PUFAs exert important neuroprotective and anti-inflammatory functions and are frequently disrupted in alcohol-related disorders [28]. Consequently, their depletion may have functional implications, potentially contributing to alcohol-related pathology through the loss of protective effects at both behavioral and molecular levels.

In addition, the depletion of PUFA-containing membrane lipids may also have important implications for EV structure and function. Membrane lipid unsaturation is a major determinant of bilayer organization and influences membrane flexibility, vesicle formation and cargo trafficking [29, 30]. Polyunsaturated acyl chains introduce structural disorder into lipid bilayers, increasing membrane flexibility and facilitating membrane remodeling processes, whereas their depletion promotes tighter lipid packing and reduced membrane fluidity [31, 32]. Consequently, the loss of highly unsaturated lipids in male-derived EVs may reflect both increased oxidative vulnerability and alterations in membrane biophysical properties, potentially affecting EV-mediated intercellular communication. In support of this interpretation, previous lipid ontology analyses of plasma EVs from AUD patients identified sex-specific

enrichment of membrane curvature-related properties, suggesting that alcohol-induced lipid remodeling directly influences EV membrane architecture [7].

In contrast to the depletion of highly unsaturated lipid species observed in males, female AUD patients exhibited a consistent enrichment of long-chain and polyunsaturated lipids across several lipid classes, including FAs, TGs and SMs. The increase in FA species containing 20–22 carbon atoms, together with the accumulation of highly unsaturated lipids, may reflect sex-specific differences in FA elongation, desaturation and lipid incorporation into EVs. These findings are in agreement with evidence showing that women generally display higher circulating levels of long-chain PUFAs, particularly docosahexaenoic acid (DHA), and a greater capacity to convert α-linolenic acid into long-chain n-3 PUFAs than men, a difference that has been linked to the influence of sex hormones on long-chain PUFA metabolism [33, 34]. Furthermore, recent systematic analyses have reported higher levels of several long-chain omega-3 and omega-6 PUFAs, particularly DHA, in females compared with males, highlighting fundamental sex-specific differences in FA metabolism [35]. In the context of chronic alcohol exposure, these intrinsic metabolic differences may contribute to a greater capacity to maintain or replenish long-chain and highly unsaturated lipid species, potentially attenuating the depletion of PUFA-containing lipids observed in males. Because acyl-chain length and unsaturation are major determinants of membrane organization and dynamics, the preservation of these lipid species may influence EV composition and function, potentially contributing to sex-specific biological responses and clinical manifestations of AUD.

Another prominent finding of this study was the extensive remodeling of EV membrane lipids in AUD patients, affecting both sphingolipid and glycerophospholipid classes. Among sphingolipids, long-chain ceramides were generally reduced in both sexes, suggesting a common disruption of sphingolipid homeostasis associated with chronic alcohol exposure. However, clear sex-dependent differences were also evident, with saturated ceramides increasing in males while decreasing in females, and polyunsaturated SMs showing the opposite pattern. Ceramides are key mediators of exosome biogenesis through the sphingomyelinase-dependent pathway, facilitating membrane curvature and inward budding of intraluminal vesicles within multivesicular bodies [36]. Based on this established role, structural remodeling of ceramide species may directly influence EV formation and cargo sorting by modifying membrane biophysical properties. In parallel, female enrichment of polyunsaturated SM species may contribute to the maintenance of membrane flexibility and structural adaptability. Since sphingomyelins are major constituents of membrane microdomains and lipid rafts, alterations in their acyl-chain composition can influence membrane packing, receptor organization and signal transduction processes [30, 37].

Extensive remodeling was also observed in membrane glycerophospholipids, including phosphatidylcholine (PC), phosphatidylethanolamine (PE) and lysophosphatidylcholine (LPC) species. Both sexes exhibited a reduction in PC species containing 34–40 total carbons, whereas PE species displayed opposite sex-dependent patterns and long-chain LPC species accumulated predominantly in males. Because PCs constitute major structural phospholipids of EV membranes, changes in their acyl-chain composition can substantially influence membrane packing, fluidity and permeability [38]. In

addition, variations in the relative abundance of PE and LPC species may affect membrane curvature and dynamics owing to their distinct molecular geometries. PE species possess a cone-shaped structure that favors membrane bending, vesicle budding and fusion events, whereas LPCs exert opposing biophysical effects through their inverted-cone shape and their ability to alter membrane tension and membrane remodeling processes [30, 38, 39]. Consequently, the coordinated redistribution of PC, PE and LPC species observed in AUD-derived EVs may influence membrane curvature dynamics and affect key processes involved in EV biogenesis, cargo sorting and uptake by recipient cells.

Several limitations should be considered when interpreting these findings. First, the relatively small sample size may have limited the detection of more subtle lipid alterations and may affect the generalizability of the results. Second, the LC-MS/MS approach used in this study enabled lipid identification primarily at the level of total carbon number and degree of unsaturation, without systematically resolving finer structural features such as double-bond position, acyl-chain distribution, or lipid isomerism. Future studies employing higher-resolution structural lipidomics will be necessary to further characterize these molecular features. Finally, although the observed changes reveal clear shifts in the structural characteristics of several lipid classes, their functional implications remain speculative. While differences in lipid chain length and unsaturation may influence EV membrane organization, biogenesis, and intercellular communication, these mechanisms were not directly assessed in the present study. Therefore, the proposed links between lipid remodeling and EV function should be considered biologically plausible hypotheses requiring further experimental validation.

Conclusions

This study reveals that chronic alcohol consumption appears to be associated with a pronounced, sex-dependent remodeling of the EV lipidome, affecting acyl-chain length, unsaturation degree and overall membrane lipid composition. These structural changes differed markedly between sexes and across lipid classes. Males showed a consistent depletion of long-chain and highly unsaturated species in FA and TG along with a more heterogeneous, class-specific pattern in glycerophospholipids. Females, in contrast, displayed a broader enrichment of long-chain and polyunsaturated lipids across several lipid categories. These changes also encompassed substantial shifts in sphingolipid and glycerophospholipid classes, which are lipid families known to shape EV stability, biodistribution and intercellular signaling. Taken together, these results position sex as a key modulator of alcohol-related lipid dysregulation and reinforce the potential of EV lipid profiles as biomarkers and mechanistic readouts of AUD pathophysiology.

Declarations

Ethics approval and consent to participate

Human plasma samples were used in accordance with the Declaration of Helsinki and were approved by the Ethics Committee of the University Hospital of Salamanca (March 2010, Project ID: PI, PI10/01692-

3/2010), and written informed consent was obtained from each participant.

Consent for publication

Not applicable.

Competing interests

The authors declare that they have no competing interests.

Funding

This work has been supported by grants from the Spanish Ministry of Health-PNSD (2023-I024), GVA (CIAICO/2024/122), the Primary Addiction Care Research Network (RD21/0009/0005 and RD24/0003/0017), FEDER Funds, GVA and the Instituto de Salud Carlos III (ISCIII) through the project PI20/00743, co-funded by the European Union and the Junta de Castilla y León (GRS 2916/A1/2023), PID2023-146865OB-I00 funded by MCIN/AEI/10.13039/501100011033/FEDER.

Author Contribution

B.M.U. analyzed the data; B.M.U. and M.P. designed and supervised the bioinformatics analysis; M.M. obtained human plasma samples and collected clinical data; B.M.U. designed and implemented the web tool; B.M.U. and M.P. wrote the manuscript; B.M.U. and M.P. designed the graphical abstract; B.M.U. and M.P. helped in the interpretation of the results; B.M.U., M.M. and M.P. writing-review and editing; M.P. conceived the work. All authors have read and approved the final manuscript.

Acknowledgement

The authors thank the Genomics and Proteomics Unit at the University of Alicante, and the Electron Microscopy Service at the Príncipe Felipe Research Centre.

Data Availability

The datasets generated and analyzed during the current study and programming scripts are available in the GitHub repository, https://github.com/Blancamartinurdiales/The-plasma-EVs-lipidome-reveals-sex-specific-acyl-chain-signatures-in-patients-with-AUD, and in a web platform: https://bioinfouvcipf.shinyapps.io/EVLipoStruct-AUD/.

References

1. Wolstenholme JT, Duong NK, Brocato ER, Bajaj JS. Gut-Liver-Brain Axis and Alcohol Use Disorder: Treatment Potential of Fecal Microbiota Transplantation. Alcohol Res. 2024;44:01. https://doi.org/10.35946/arcr.v44.1.01.
2. Ayares G, Idalsoaga F, Arnold J, Fuentes-López E, Arab JP, Díaz LA. Public Health Measures and Prevention of Alcohol-Associated Liver Disease. J Clin Exp Hepatol. 2022;12:1480–91. https://doi.org/10.1016/j.jceh.2022.05.005.
3. Shao H, Im H, Castro CM, Breakefield X, Weissleder R, Lee H. New Technologies for Analysis of Extracellular Vesicles. Chem Rev. 2018;118:1917–50. https://doi.org/10.1021/acs.chemrev.7b00534.
4. Frühbeis C, Fröhlich D, Kuo WP, Krämer-Albers E-M. Extracellular vesicles as mediators of neuron-glia communication. Front Cell Neurosci. 2013;7:182. https://doi.org/10.3389/fncel.2013.00182.
5. Cho Y-E, Song B-J, Akbar M, Baek M-C. Extracellular vesicles as potential biomarkers for alcohol- and drug-induced liver injury and their therapeutic applications. Pharmacol Ther. 2018;187:180–94. https://doi.org/10.1016/j.pharmthera.2018.03.009.
6. Perpiñá-Clérigues C, Mellado S, Català-Senent JF, Ibáñez F, Costa P, Marcos M, et al. Lipidomic landscape of circulating extracellular vesicles isolated from adolescents exposed to ethanol intoxication: a sex difference study. Biol Sex Differ. 2023;14:22. https://doi.org/10.1186/s13293-023-00502-1.
7. Perpiñá-Clérigues C, Mellado S, Galiana-Roselló C, Fernández-Regueras M, Marcos M, García-García F, et al. Novel insight into the lipid network of plasma extracellular vesicles reveal sex-based differences in the lipidomic profile of alcohol use disorder patients. Biol Sex Differ. 2024;15:10. https://doi.org/10.1186/s13293-024-00584-5.
8. Rose TD, Köhler N, Falk L, Klischat L, Lazareva OE, Pauling JK. Lipid network and moiety analysis for revealing enzymatic dysregulation and mechanistic alterations from lipidomics data. Brief Bioinform. 2023;24:bbac572. https://doi.org/10.1093/bib/bbac572.
9. Han X, Gross RW. The foundations and development of lipidomics. J Lipid Res. 2022;63:100164. https://doi.org/10.1016/j.jlr.2021.100164.
10. Pinto SN, Silva LC, Futerman AH, Prieto M. Effect of ceramide structure on membrane biophysical properties: The role of acyl chain length and unsaturation. Biochimica et Biophysica Acta (BBA). - Biomembr. 2011;1808:2753–60. https://doi.org/10.1016/j.bbamem.2011.07.023.
11. Maula T, Al Sazzad MA, Slotte JP. Influence of Hydroxylation, Chain Length, and Chain Unsaturation on Bilayer Properties of Ceramides. Biophys J. 2015;109:1639–51. https://doi.org/10.1016/j.bpj.2015.08.040.
12. Akerele OA, Cheema SK. Fatty acyl composition of lysophosphatidylcholine is important in atherosclerosis. Med Hypotheses. 2015;85:754–60. https://doi.org/10.1016/j.mehy.2015.10.013.
13. Kihara A. Very long-chain fatty acids: elongation, physiology and related disorders. J Biochem. 2012;152:387–95. https://doi.org/10.1093/jb/mvs105.

14. Mellado S, Morillo-Bargues MJ, Perpiñá-Clérigues C, García-García F, Moreno-Manzano V, Guerri C, et al. The emerging role of mesenchymal stem cell–derived extracellular vesicles to ameliorate hippocampal NLRP3 inflammation induced by binge-like ethanol treatment in adolescence. Neural Regeneration Res. 2025;20:1153. https://doi.org/10.4103/NRR.NRR-D-23-01397.
15. Koelmel JP, Li X, Stow SM, Sartain MJ, Murali A, Kemperman R, et al. Lipid Annotator: Towards Accurate Annotation in Non-Targeted Liquid Chromatography High-Resolution Tandem Mass Spectrometry (LC-HRMS/MS) Lipidomics Using a Rapid and User-Friendly Software. Metabolites Multidisciplinary Digit Publishing Inst. 2020;10:101. https://doi.org/10.3390/metabo10030101.
16. Tsugawa H, Cajka T, Kind T, Ma Y, Higgins B, Ikeda K, et al. MS-DIAL: data-independent MS/MS deconvolution for comprehensive metabolome analysis. Nat Methods Nat Publishing Group. 2015;12:523–6. https://doi.org/10.1038/nmeth.3393.
17. Sartain M, Van de Bittner G, Stow S. Lipid Profiling Workflow Demonstrates Disrupted Lipogenesis Induced with Drug Treatment in Leukemia Cells. Combined with Lipid Annotator and 6546 LC/Q-TOF. Agilent Application Note. 2020;5994–en1356.
18. Mohamed A, Molendijk J, Hill MM. J Proteome Res Am Chem Soc. 2020;19:2890–7. https://doi.org/10.1021/acs.jproteome.0c00082. lipidr: A Software Tool for Data Mining and Analysis of Lipidomics Datasets.
19. Benjamini Y, Hochberg Y. Controlling the False Discovery Rate: A Practical and Powerful Approach to Multiple Testing. J Roy Stat Soc: Ser B (Methodol). 1995;57:289–300. https://doi.org/10.1111/j.2517-6161.1995.tb02031.x.
20. Sud M, Fahy E, Cotter D, Azam K, Vadivelu I, Burant C, et al. Metabolomics Workbench: An international repository for metabolomics data and metadata, metabolite standards, protocols, tutorials and training, and analysis tools. Nucleic Acids Res. 2016;44:D463–470. https://doi.org/10.1093/nar/gkv1042.
21. Fahy E, Subramaniam S. RefMet: a reference nomenclature for metabolomics. Nat Methods Nat Publishing Group. 2020;17:1173–4. https://doi.org/10.1038/s41592-020-01009-y.
22. Sud M, Fahy E, Cotter D, Brown A, Dennis EA, Glass CK, et al. LMSD: LIPID MAPS structure database. Nucleic Acids Res. 2007;35:D527–32. https://doi.org/10.1093/nar/gkl838.
23. Martín-Urdiales B, Perpiñá-Clérigues C, Mellado S, Rojas-Pirela M, Aguilar Sánchez M-L, Puertas-Miranda D, et al. Deciphering Lipidomics Landscape of Urine Extracellular Vesicles in Alcohol Use Disorder Patients. J Proteome Res. 2025;24:5653–63. https://doi.org/10.1021/acs.jproteome.5c00515.
24. Perpiñá-Clérigues C, Mellado S, Galiana-Roselló C, García-García F, Pascual M. Unraveling the Impact of TLR4 and Sex on Chronic Alcohol Consumption-Induced Lipidome Dysregulation in Extracellular Vesicles. J Proteome Res. 2025;24:1197–208. https://doi.org/10.1021/acs.jproteome.4c00786.
25. Prokopieva VD, Vetlugina TP. Features of oxidative stress in alcoholism. Biomed Khim. 2023;69:83–96. https://doi.org/10.18097/PBMC20236902083.

26. Viola TW, Orso R, Florian LF, Garcia MG, Gomes MGS, Mardini EM, et al. Effects of substance use disorder on oxidative and antioxidative stress markers: A systematic review and meta-analysis. Addict Biol. 2023;28:e13254. https://doi.org/10.1111/adb.13254.
27. Islam F, Imran A, Nosheen F, Fatima M, Arshad MU, Afzaal M, et al. Functional roles and novel tools for improving-oxidative stability of polyunsaturated fatty acids: A comprehensive review. Food Sci Nutr. 2023;11:2471–82. https://doi.org/10.1002/fsn3.3272.
28. Cardona D, Carvajal F, Lerma-Cabrera JM, Sánchez-Gil A, Rueda-Ruzafa L. Impact of Omega-3 Polyunsaturated Fatty Acids on Alcohol Use and Negative Consequences: A Systematic Review. Nutr Rev. 2025;83:1214–26. https://doi.org/10.1093/nutrit/nuaf036.
29. Ghadami S, Dellinger K. The lipid composition of extracellular vesicles: applications in diagnostics and therapeutic delivery. Front Mol Biosci. 2023;10:1198044. https://doi.org/10.3389/fmolb.2023.1198044.
30. Skotland T, Sagini K, Sandvig K, Llorente A. An emerging focus on lipids in extracellular vesicles. Adv Drug Deliv Rev. 2020;159:308–21. https://doi.org/10.1016/j.addr.2020.03.002.
31. Harayama T, Antonny B. Beyond Fluidity: The Role of Lipid Unsaturation in Membrane Function. Cold Spring Harb Perspect Biol. 2023;15:a041409. https://doi.org/10.1101/cshperspect.a041409.
32. Kim K-H, Yoo BC. Decoding Membrane Lipids: Analytical Barriers and Technological Advances in Modern Lipidomics. Int J Mol Sci. 2026;27:1472. https://doi.org/10.3390/ijms27031472.
33. Burdge GC, Wootton SA. Conversion of alpha-linolenic acid to eicosapentaenoic, docosapentaenoic and docosahexaenoic acids in young women. Br J Nutr. 2002;88:411–20. https://doi.org/10.1079/BJN2002689.
34. Decsi T, Kennedy K. Sex-specific differences in essential fatty acid metabolism. Am J Clin Nutr. 2011;94. https://doi.org/10.3945/ajcn.110.000893. :1914S-1919S.
35. Li D, Shum C, Khoo A, Shi T, Green MR, Blanco Mejia S, et al. Sex Differences in Omega-3 and Omega-6 PUFA Status: A Systematic Review and Meta-analysis of Cross-Sectional Comparisons. Adv Nutr. 2026;17:100670. https://doi.org/10.1016/j.advnut.2026.100670.
36. Trajkovic K, Hsu C, Chiantia S, Rajendran L, Wenzel D, Wieland F, et al. Ceramide triggers budding of exosome vesicles into multivesicular endosomes. Volume 319. New York, N: Science; 2008. pp. 1244–7. https://doi.org/10.1126/science.1153124.
37. Slotte JP. Biological functions of sphingomyelins. Prog Lipid Res. 2013;52:424–37. https://doi.org/10.1016/j.plipres.2013.05.001.
38. Harayama T, Riezman H. Understanding the diversity of membrane lipid composition. Nat Rev Mol Cell Biol. 2018;19:281–96. https://doi.org/10.1038/nrm.2017.138.
39. Kozlov MM, Taraska JW. Generation of nanoscopic membrane curvature for membrane trafficking. Nat Rev Mol Cell Biol Nat Publishing Group. 2023;24:63–78. https://doi.org/10.1038/s41580-022-00511-9.

Figures

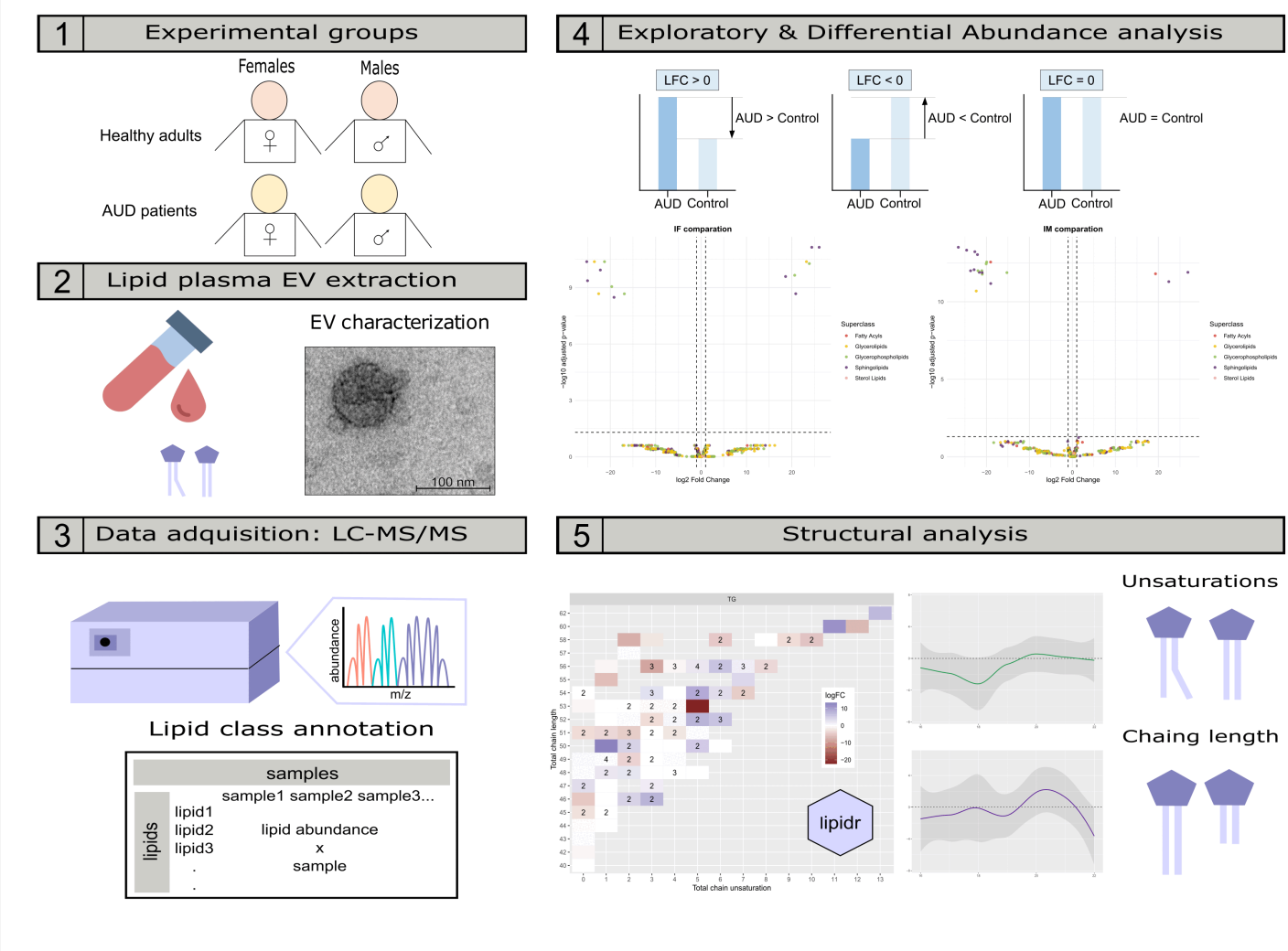


Figure 1

Experimental design and structural lipidomic workflow. Plasma extracellular vesicles (EVs) were isolated from male and female patients with alcohol use disorder (AUD) and healthy individuals (controls). Lipids were extracted, quantified, and identified using LC-MS/MS. Following data normalization and lipid class annotation, differential abundance analyses were performed to evaluate lipid abundance. Structural lipidomic analyses were conducted using the *lipidr*package to assess the total number of unsaturated bonds and the total chain length (carbon number) in lipid classes of interest from plasma EVs of AUD patients and controls.

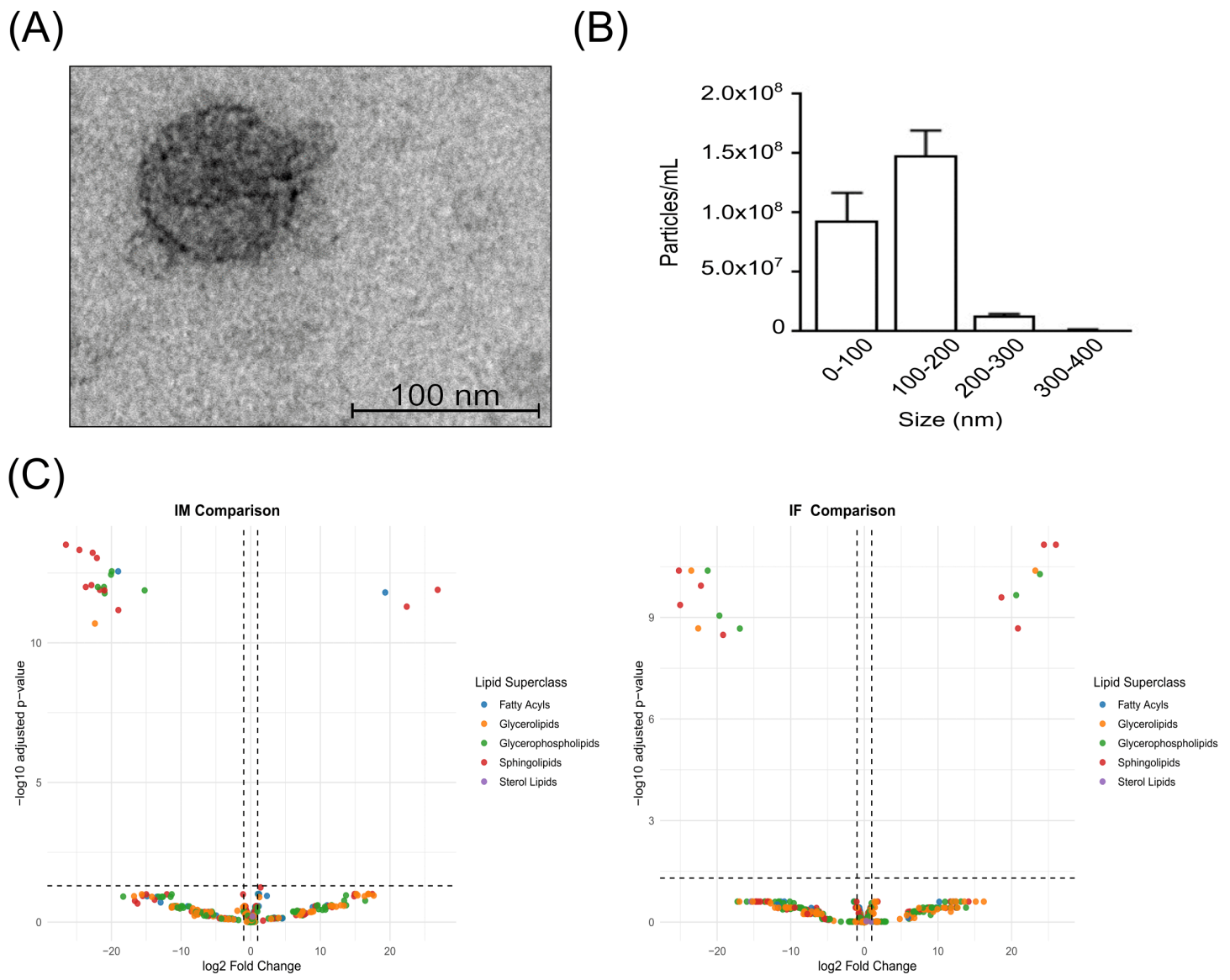


Figure 2

Characterization of plasma extracellular vesicles. A) Transmission electron microscopy (TEM) micrograph showing isolated human plasma extracellular vesicles (EVs). **B)** Nanoparticle tracking analysis (NTA) displaying the size distribution and concentration of plasma EV particles. **C)** Volcano plots representing lipid alterations in the IM (Impact of AUD in Males) and IF (Impact of AUD in Females) comparisons, with lipids colored according to lipid superclass.

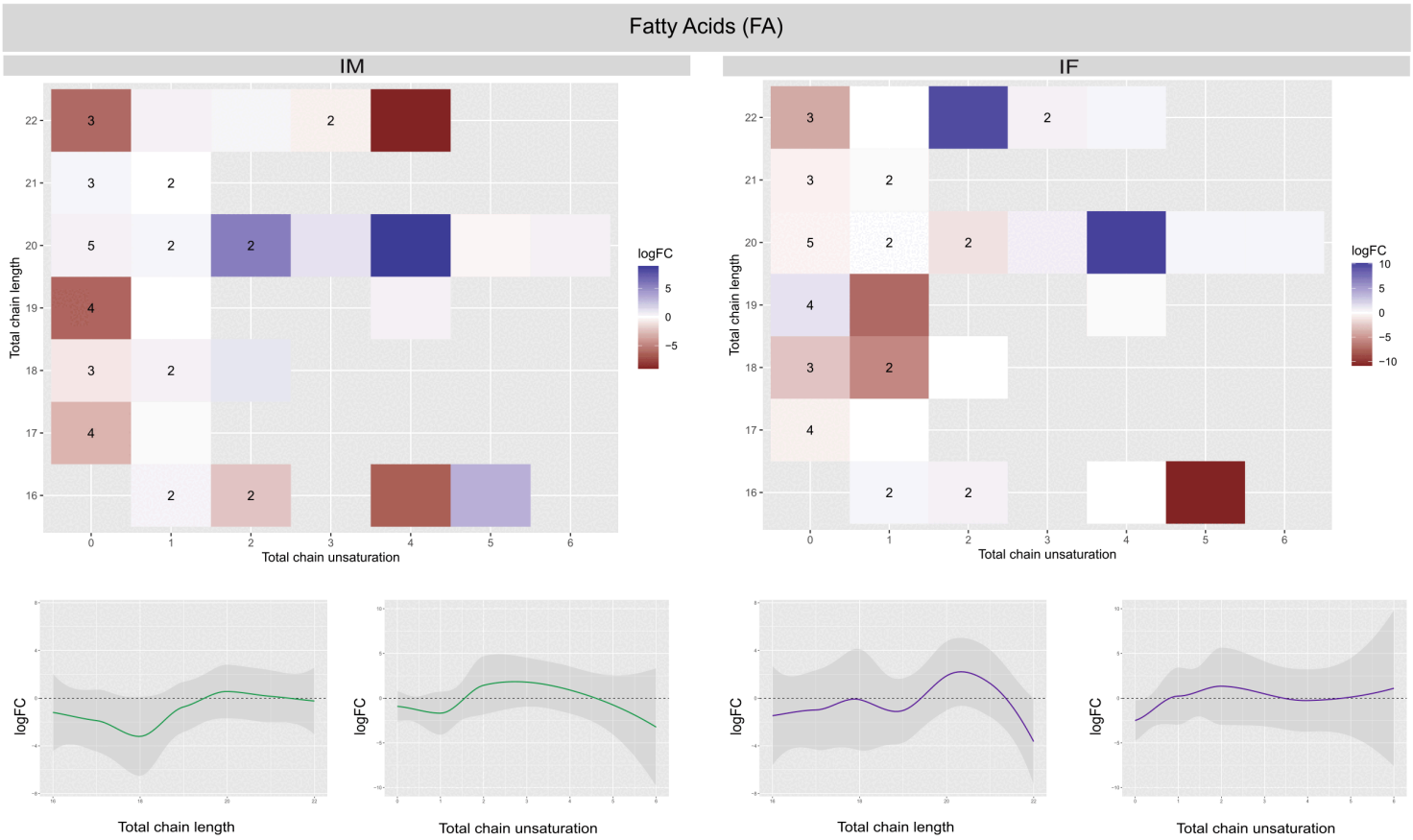


Figure 3

Sex-stratified differential structural patterns in fatty acids (FA).
The figure presents results for the fatty acid (FA) lipid class. Comparisons are stratified by sex, with males (IM) on the left and females (IF) on the right. The upper panels display chain distribution plots, where abundance changes (LFC) of individual FA species are summarized according to total carbon chain length and degree of unsaturation. When multiple lipid species share the same structural features, values are averaged and the number of contributing molecules is indicated. The lower panels show trend analyses, including linear regression of LFC against total chain length (left) and total number of double bonds (right), highlighting global structural patterns associated with the comparison.

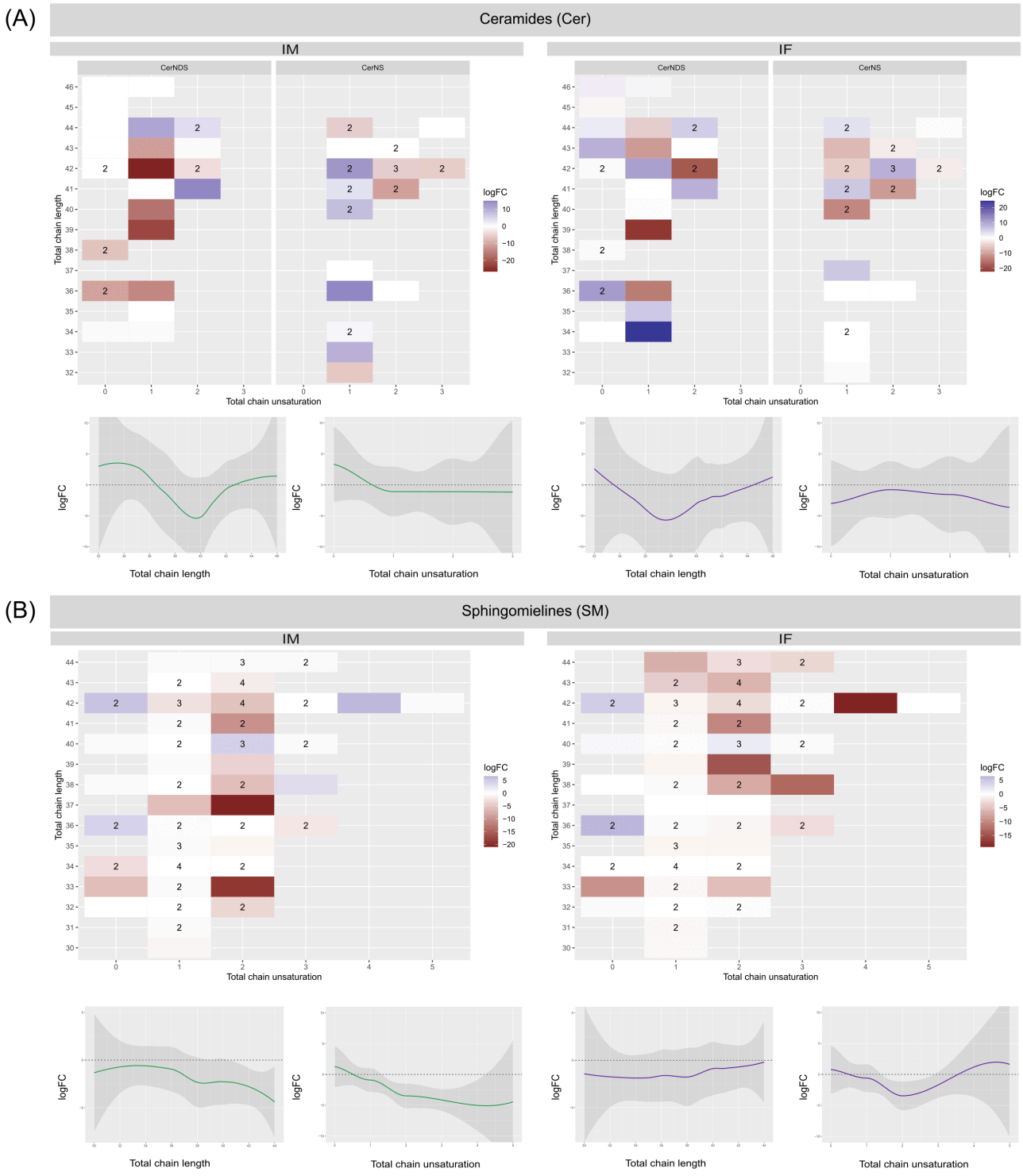


Figure 4

Sex-stratified differential structural patterns in sphingolipids (SPL).

The figure presents results for sphingolipids classes analyzed separately: **A)**ceramides (Cer) and **B)** sphingomielines (SM). Comparisons are stratified by sex, with males (IM) on the left and females (IF) on the right. The upper panels display chain distribution plots, where abundance changes (LFC) of individual lipid species are summarized according to total carbon chain length and degree of unsaturation. When

multiple lipid species share the same structural features, values are averaged and the number of contributing molecules is indicated. The lower panels show trend analyses, including linear regression of LFC against total chain length (left) and total number of double bonds (right), highlighting global structural patterns associated with each comparison.

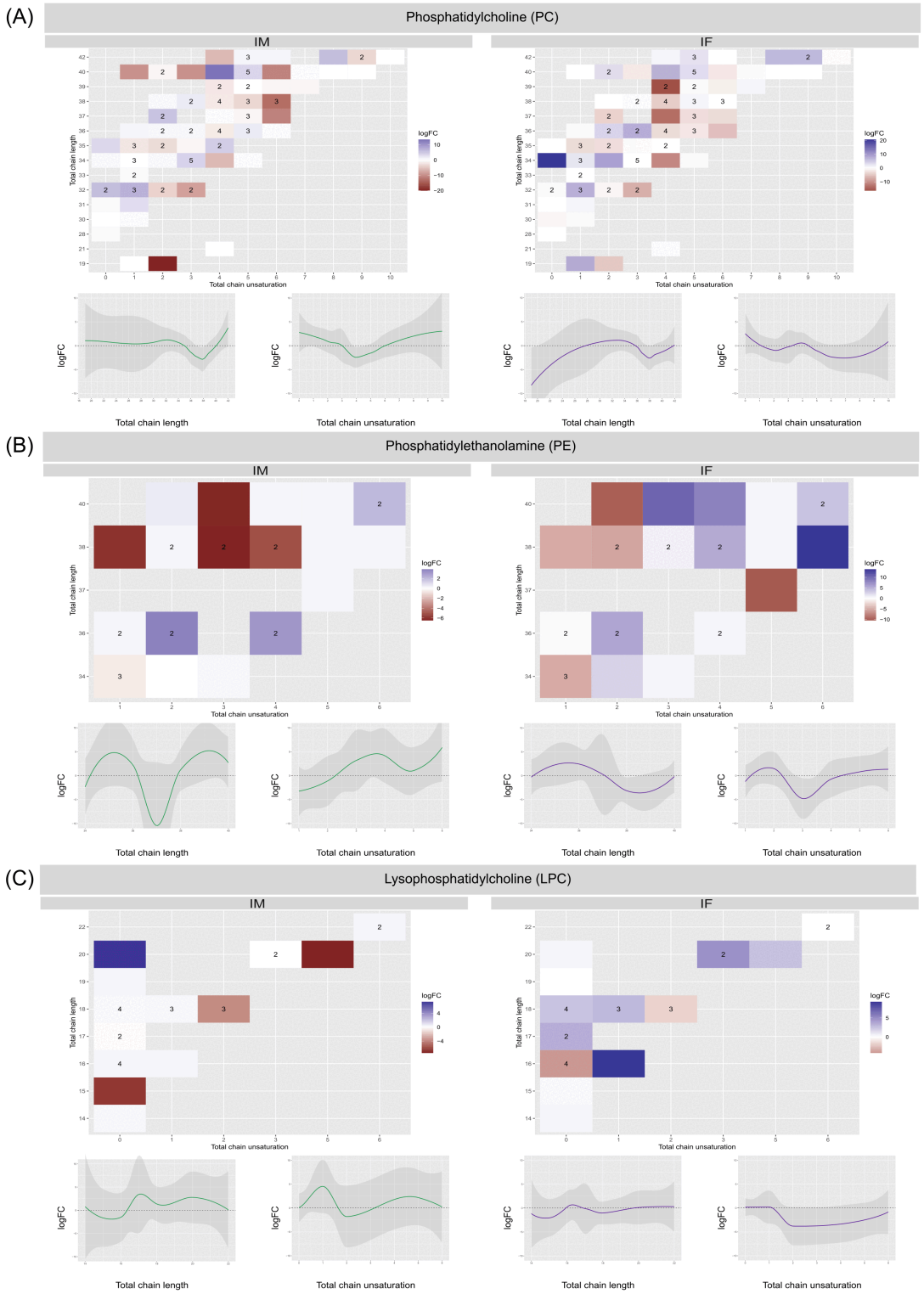


Figure 5

Sex-stratified differential structural patterns in phospholipids (PL).
The figure presents results for phospholipid subclasses analyzed separately: **A)**phosphatidylcholines (PC), **B)** phosphatidylethanolamines (PE), and **C)**lysophosphatidylcholines (LPC). Comparisons are stratified by sex, with males (IM) on the left and females (IF) on the right. The upper panels display chain distribution plots, where abundance changes (LFC) of individual lipid species are summarized according to total carbon chain length and degree of unsaturation. When multiple lipid species share the same structural features, values are averaged and the number of contributing molecules is indicated. The lower panels show trend analyses, including linear regression of LFC against total chain length (left) and total number of double bonds (right), highlighting global structural patterns associated with each comparison.

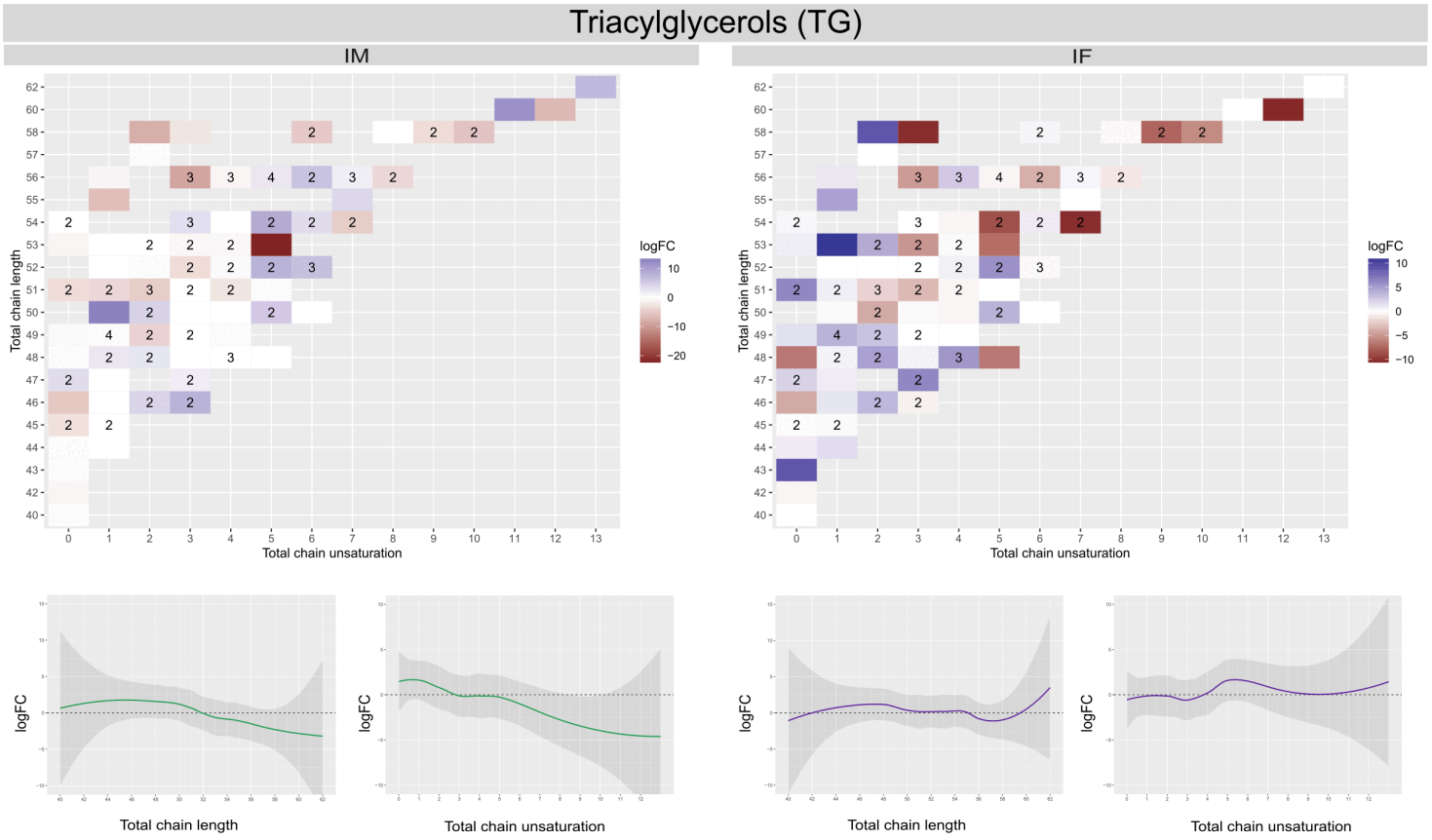


Figure 6

Sex-stratified differential structural patterns in triacylglycerols (TG).
The figure presents results for the triacylglycerols (TG) lipid class. Comparisons are stratified by sex, with males (IM) on the left and females (IF) on the right. The upper panels display chain distribution plots, where abundance changes (LFC) of individual TG species are summarized according to total carbon chain length and degree of unsaturation. When multiple lipid species share the same structural features, values are averaged and the number of contributing molecules is indicated. The lower panels show trend analyses, including linear regression of LFC against total chain length (left) and total number of double bonds (right), highlighting global structural patterns associated with the comparison.

Supplementary Files

This is a list of supplementary files associated with this preprint. Click to download.

- SupplementaryMaterialAUD.docx
- OnlineGraphicalabstract.png